

How to Cite:

Alshujery, M. K., & Al-Saadie, K. A. S. (2022). Anodizing of aluminum 6061 alloy with incorporated nanoparticles to inhibits the aluminum corrosion. *International Journal of Health Sciences*, 6(S1), 930-940. <https://doi.org/10.53730/ijhs.v6nS1.4847>

Anodizing of Aluminum 6061 Alloy with Incorporated Nanoparticles to Inhibits the Aluminum Corrosion

Mohannad Kadhim Alshujery

Department of Chem., College of Science, Baghdad University, Baghdad, Iraq

Khulood Abid Saleh Al-Saadie

Department of Chem., College of Science, Baghdad University, Baghdad, Iraq

Abstract--In this work, Aluminum alloy 6061 (A6061) was modified by Anodizing and incorporating with ZnO and Fe₃O₄ nanoparticles to improve its corrosion-resistant. The titanium sheet was used as a counter electrode and the DC voltage reach 20 mV while the anodizing solution was 20% H₂SO₄ while the H₂SO₄ was mixed with the two Oxide nanoparticle to incorporate the AA6061 surface. Anodizing and incorporation with (ZnO and Fe₃O₄) NPS were confirmed by X-ray diffraction. The surface morphology of anodized and incorporated surface was examined through scanning electron microscopy (SEM). Modified A6061 by Anodizing and nanoparticle incorporation revealed a good corrosion protection efficiency even at temperatures ranging (298-328) K in a saline medium. Where the corrosion current density increase with the increase in temperature. Activation energy and pre-exponential factor (kinetic parameters) were calculated and discussed. Also, thermodynamic values? G* and? H* were calculated.

Keywords---aluminum, anodizing, incorporated, kinetic parameters, nanoparticles.

Introduction

Aluminum alloy 6061 (A6061) is an aluminum alloy with primary alloying components magnesium and silicon. A6061 has superior corrosion resistance, machinability, weldability, and anodizing response due to the alloying elements used (1, 2). It is widely employed in a variety of applications, including home structures, cell phone cases, and automobiles (3, 4). Even though A6061 has high corrosion resistance, corrosion sometimes occurs due to intermetallic particles in the alloy. As a result, varieties of surface treatments are often utilized to preserve the alloy from corrosion. One of them is anodizing. Electrochemical processes

International Journal of Health Sciences ISSN 2550-6978 E-ISSN 2550-696X © 2022.

Corresponding author: Alshujery, M. K.

Manuscript submitted: 27 Nov 2021, Manuscript revised: 18 Feb 2022, Accepted for publication: 09 March 2022

produce anodic aluminum oxide (AAO) coating on the surface during the anodizing process (5). The anodic aluminum oxide (AAO) film has two layers: an inner barrier layer and an outer porous layer. Because of its compact dense structure, the inner barrier layer plays an essential role in corrosion resistance. The outer porous layer is composed of hexagonal cells with a single cylindrical pore in the middle of each cell, resulting in its absorption characteristic (6). As a result, numerous qualities, such as good interface adhesion, good surface appearance, and enhancement of mechanical and anti-corrosive capabilities, maybe enhanced after anodizing (7). In general, the anodizing process mainly consists of three parts. The first step is surface preparation, which is used to manage the surface's quality. The second stage is anodizing, which creates an anodic oxide coating, and the last step is sealing, which closes up oxide pores. major processes have been patented to achieve an anodized aluminum surface (8). the nanoparticle incorporated by adding it with anodizing solution, Soaking anodized aluminum into a suspension mixture containing nanoparticles this method provides pore sealing layer distributed with nanoparticles (9, 10).

The precise control of the size of nanoparticles in the suspension is needed and aggregation of nanoparticles must be avoided. In this work, we have proposed a new method to modify the surface of A6061 by using the electrochemical method of Anodizing and incorporating nanoparticles simultaneously into the porous layer of Anodized Aluminum 6061 (AA6061). This process is carried out during the anodizing process. Study the Effects of Anodized Aluminum 6061 in the presence of ZnO (AA6061+ZnO)and Anodized Aluminum 6061in presence of Fe₃O₄ (AA6061+Fe₃O₄).

Experimental part

Before anodization, Aluminum specimens have a diameter of 2.5 cm² and a thickness of 0.5 mm were produced by press cutting of commercially high purity A6061 sheet. The samples were polished with a different emery paper with grit 600, 800, 1000, 1200, and 2000, and then it was polished to a semi-mirror. After polishing the samples were washed with distilled water and placed in an ultrasonic bath with acetone for five minutes, then rinsed with distilled water, dried, and finally kept in a desiccator. Then the aluminum samples were treated by immersing them in 10% NaOH for 30 seconds to oxidize the surface, followed by a rinse with distilled water to remove the sodium hydroxide remnants, and the oxidized layer was removed by immersing in 50% HNO₃ until the black oxide layer was removed. Finally, the samples were rinsed with distilled water to remove the acid residue and prepare them for anodizing.

The anodizing process was carried out in the anodizing cell represented in figure.1; the anodizing process was performed under a constant voltage (20 volts) for 30 minutes. Using a DC power supply, in which the large titanium foil counter electrode was employed. The electrodes were immersed in a 20% sulfuric acid solution with an inter-electrode spacing of up to 4 cm. To incorporate nanoparticles (ZnO and Fe₃O₄) in Aluminum oxide nanopores formed during the anodizing process, 0.1wt% nanoparticles were added to sulfuric acid. After the anodizing process with and without nanoparticles finishing, samples were removed, rinsed with cold distilled water then immersed in boiled water for two

minutes (to seal the nanopores), dried, and placed in containers to be tested later. The morphologies of the treated aluminum were observed by field emission scanning electron microscopy (FE-SEM) and the chemical composition of samples were measured by X-ray diffraction (XRD).

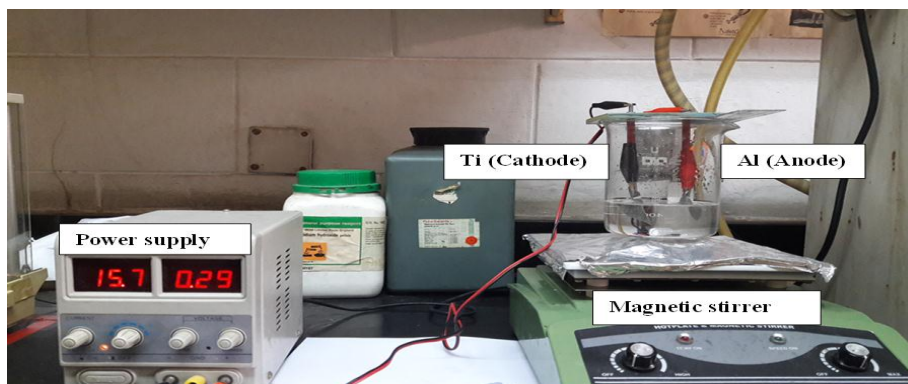


Figure 1. Shows a picture of an anodizing cell and illustrates its components

A WENKING M Lab. (Germany) equipment was used to measure the polarization. Polarization curves for A6061 were obtained before and after anodizing. The working, counter, and reference electrodes were A6061, Pt, and Ag/AgCl (sat. KCl (aq)), respectively. As a corrosive medium, saline (3.5% NaCl) solutions were applied.

Results and Discussion

Chemical structure and morphology of oxide layer:

The FESEM and XRD techniques showed the morphology and chemical structures of the oxide layer formed on A6061 with and without nanoparticles incorporated in the nanopore, respectively (Figure 2 and Figure 3). During the anodizing processes of all samples (A6061, AA6061+ZnO, and AA6061+Fe₃O₄) at the applied 20 voltage and kept constant for 30 min. In the absence of nanoparticles, a layer of aluminum oxide with non-uniform micropores was formed on the surface of the anodized sample (AA6061), where the diameter of formed pores was 215 nm while the average particle size of particle oxide was 35 nm, (Figure 2a). It was observed that by adding ZnO and Fe₃O₄ nanoparticles to the electrolytes of the AA6061+ZnO and AA6061+Fe₃O₄ samples (Figure 2b & 2c).

Nanoparticles were distributed throughout the surfaces of these oxide layers, filling the majority of the micropores. Furthermore, as can be shown, the majority of these integrated nanoparticles are not recognizable and are detected with a size bigger than their main diameter. Indeed, the electrophoretic force attracts nanoparticles to the surface of the sample (anode) and causes them to cover the surface and fill the micropores of the coatings.

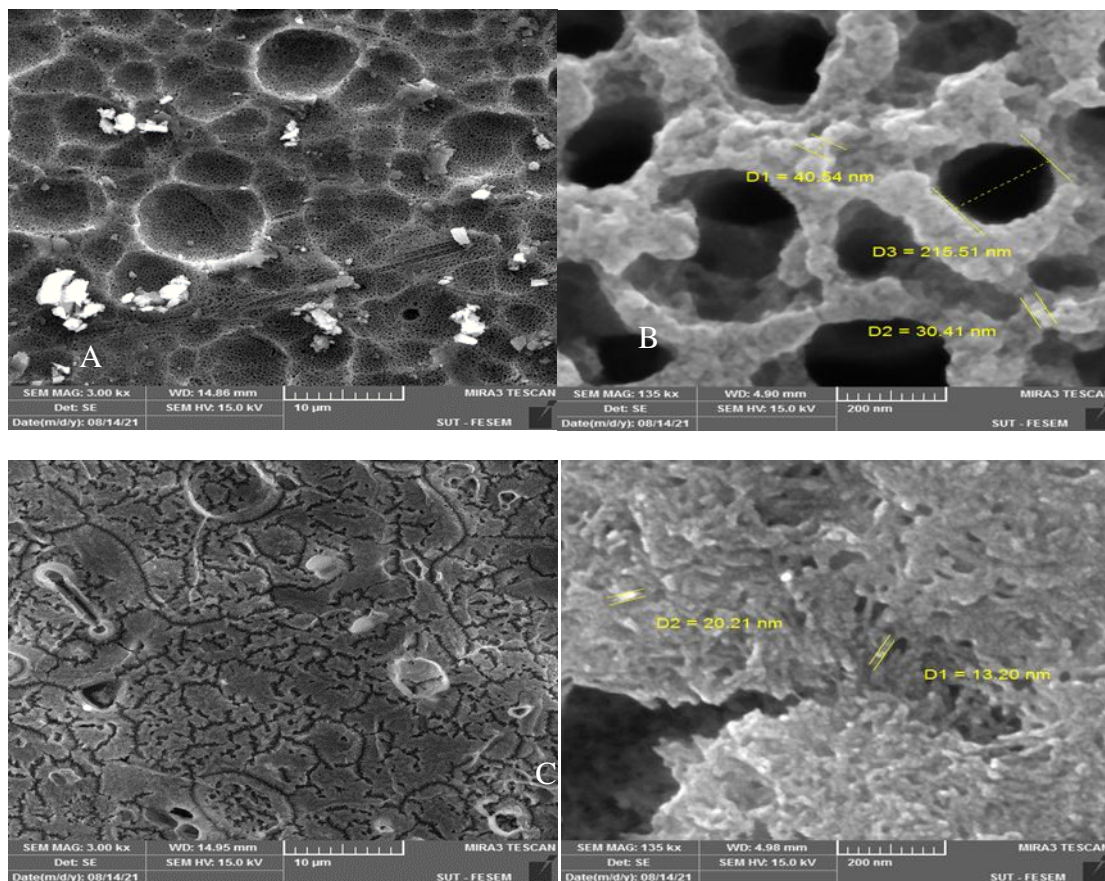


Figure 2. Shows Surface morphologies as seen via a FESEM of A) AA6061, B) AA6061+ZnO, and C) AA6061+Fe₃O₄ samples in ×3000 and ×135000 magnifications

The X-ray diffraction features of the Anodized aluminum oxide and the incorporated ZnO and Fe₃O₄ formed on A6061 by Anodizing method are shown in Figure 3. The phases may be seen in all of the XRD patterns. Furthermore, due to the thinness of the oxide layer, the matching peaks to the aluminum substrate were identified in all XRD spectrums. However, peaks of Al₂O₃ (the oxide of the A6061 substrate) were found in these patterns. The average particle size of incorporated nanoparticles induced using the current electrochemical process may be calculated using Debye–approximation Scherrer's from the peaks' full width at half maximum (FWHM). (Eq. 1) (11).

$$d = k\lambda / \beta \cos\theta \quad \dots (1)$$

Where d is the crystallite size, k is the CuK α radiation wavelength ($k = 1.542\text{\AA}$), β is the FWHM for the diffraction peak in concern (in radians), θ is the diffraction angle, and k is the broadening constant ($k=0.9$). The small peaks at 2θ (38° , 42° , and 65°) referred to γ -Al₂O₃. The crystallite size has been detected for Al₂O₃ formed on AA6061 without nanoparticles and has an average size equal to (19.8 nm) (Figure 3).

The incorporation of nanoparticles slightly affects the peak positions are slightly shifted to higher 2-theta (2θ) values compared to that AA6061 without nanoparticles.

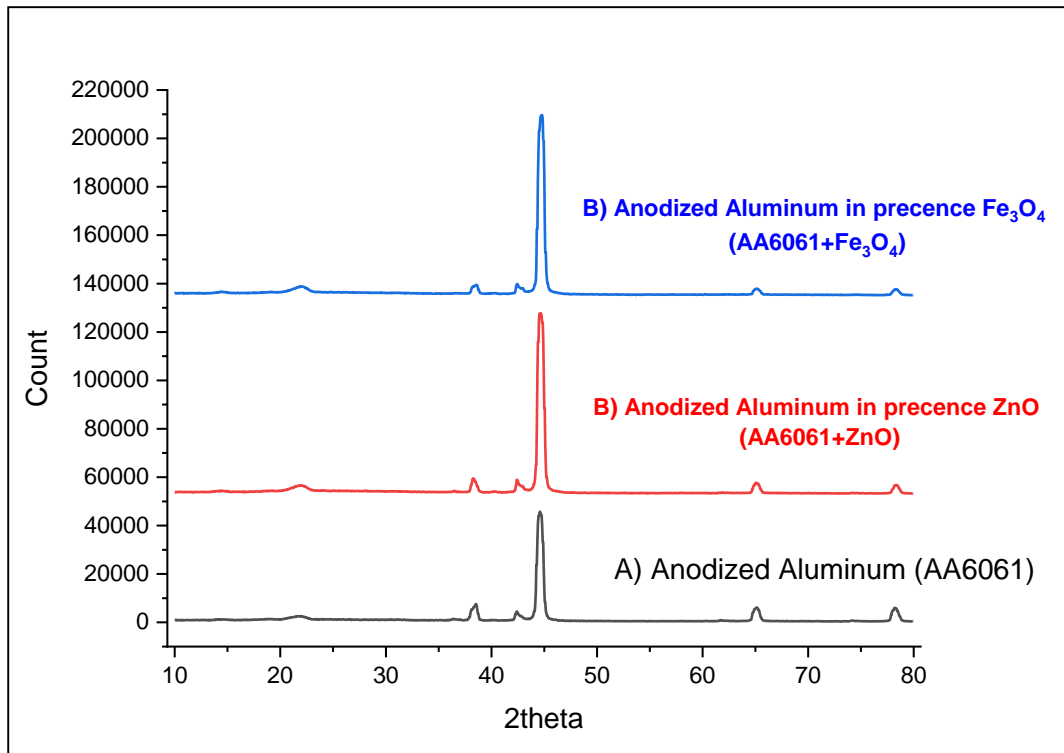
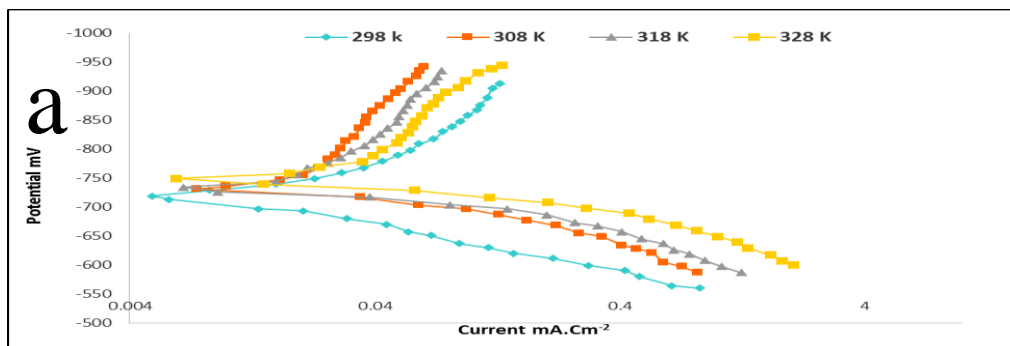


Figure 3. The XRD spectra of the anodized samples

Corrosion test

Figure (4) represents the Tafel curves for the corrosion test on A6061 with anodizing and oxide nanoparticles incorporated at various temperatures. The corrosion potential of blank A6061 is shown by the polarization curves (-718.7 to -748.7 mV). After anodizing in sulfuric acid solution the potential shifted to (-727.9 mV) at 298K, and the E_{Corr} shifted to 681.2, 693.7 after AA6061 incorporated with ZnO Nanoparticle and Fe₃O₄ respectively.



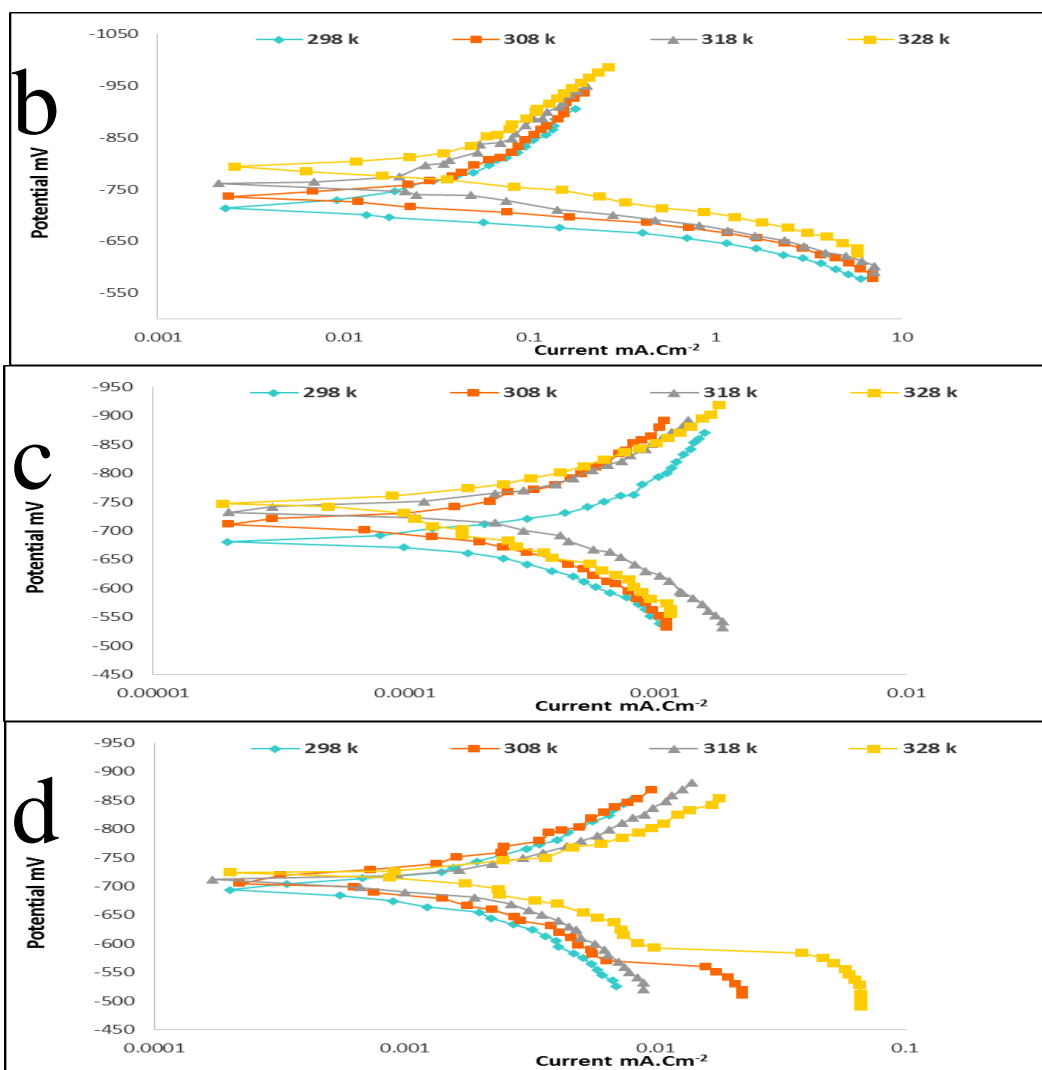


Figure.4. Polarization curves for a) Blank AA6061 (Blank), b) Anodizing AA6061 c) Anodizing + Fe_3O_4 d) Anodizing + ZnO

The corrosion current density has significantly raised as the temperature raised for Blank AA6061, but after anodizing, the corrosion current density decreased from 15.73 microamperes to 1.77 microamperes, and the I_{CORR} value decreased further to the Nanoampere value with the Nanoparticle incorporated. These results indicate that anodizing and incorporation improve the corrosion resistance of A6061. Using the equation below, the Protection Efficiency (% PE) may be computed (12).

$$\%PE = \frac{(I_{\text{CORR}})_b - (I_{\text{CORR}})_t}{(I_{\text{CORR}})_b} \times 100 \dots \dots (2)$$

Where $(I_{\text{CORR}})_b$ and $(I_{\text{CORR}})_t$ are the corrosion current density ($\mu\text{A}.\text{cm}^{-2}$) for A6061 (Blank) and treated AA6061 after anodizing respectively.

Table 1
Corrosion kinetic parameters for Protective Aluminum 6061 alloy in seawater at the temperatures range (298-328) K

Temp./K	$E_{\text{Corr}}/$ mV	$I_{\text{Corr}}/$ $\mu\text{A.c}$	b_c/m V.dec	b_a/m V.dec	$w.l/g. m^{-2}.dl^{-1}$	$P.L/$ $mm.y^{-1}$	R_p /	PE%	
un treated A6061	29	-	15.73	141.3	109.1	1.27	0.171	16	-
	30	-	20.55	476.3	57.3	1.65	0.224	10	-
	31	-	26.3	477.8	61.8	1.79	0.243	90	-
	32	-	31.83	495.6	75.8	2.56	0.346	89	-
After Anodizin g	29	-	1.77	46	29.5	0.151	0.0203	21	88.747
	30	-	3.54	68.7	33.3	0.278	0.0375	20	82.773
	31	-	4.91	60.4	36.2	0.378	0.0511	10	81.330
	32	-	8.23	49.9	39.5	0.569	0.0769	91	74.143
Anodizin g with Fe3O4	29	-	0.211	75.1	43.3	0.017	0.0023	21	98.658
	30	-	0.483	75.7	111.7	0.0247	0.00334	20	97.649
	31	-	0.711	62.3	78.6	0.0388	0.00689	10	97.296
	32	-	0.992	57.9	101.1	0.0791	0.00929	91	96.883
Anodizin g with ZnO	29	-	0.117	110	118.6	0.0124	0.00143	21	99.256
	30	-	0.193	192.2	173.4	0.0155	0.0021	20	99.060
	31	-	0.257	173.2	102.7	0.0212	0.00287	10	99.022
	32	-	0.324	115	170	0.0545	0.00441	91	98.982

The best % PE was observed after AA6061 anodizing, which gave a % PE of 88.7% at 298K; nevertheless, table (1) data reveals that % PE decreased as temperature increased, illustrating that I_{Corr} for Anodized AA6061 was affected by temperature. While the best % PE was obtained after AA6061 was incorporated with Fe_3O_4 , which gave a % PE of 98.65% percent at 298K. The best PE % was acquired with ZnO incorporation at 99.25% at 298K, the PE% for incorporated AA6061 slightly decreased with temperature increasing, indicating that I_{Corr} for incorporated AA6061 was not affected by temperature change. Near the corrosion potential E_{Corr} , there is a little amount of polarization. The following equation, known as the Stern–Geary equation, is used to determine corrosion resistance:

$$R_p = \Delta E / \Delta i = (b_a * b_c) / (2.303 * (b_a + b_c)) * 1000 \dots (3)$$

R_p is the system's polarization resistance, ΔE denotes the difference between the polarization potential E and the corrosion potential E_{Corr} , Δi denotes the difference between the observed current density I and the corrosion current density I_{Corr} , and b_a and b_c denote the anodic and cathodic Tafel coefficients, respectively. The measurement of entire polarization curves is required when discussing polarization resistance and it is especially useful in diagnosing corrosion problems and initiating reconditioning action (13).

The thermodynamic studies

The Arrhenius equation might be used to calculate the change in entropy (ΔS^*) for the transition, state of corrosion process (14):

$$\text{Log } I_{\text{corr}}/T = \log R/Nh + \Delta S^*/2.303R - \Delta H^*/2.303RT \dots\dots(4)$$

Where I_{corr} is the A6061 corrosion current density calculated from the Tafel plot, h is the Plank's constant, N is the Avogadro number, ΔS^* is the activation entropy, and ΔH^* is the activation enthalpy. The slope of $(-\Delta H^* / 2.303 R)$ and the intercept of $[(\log (R/Nh) + (\Delta S^*/2.303 R))]$ were derived from the plot of $\log I_{\text{corr}}/T$ versus $1/T$, from which the values of ΔH^* and ΔS^* , respectively, were estimated. The data in table (2) shows that after treating the surface of AA6061, the values of entropy changed slightly. Figure (5) shows the plot of $\log I_{\text{corr}}/T$ against $1/T$.

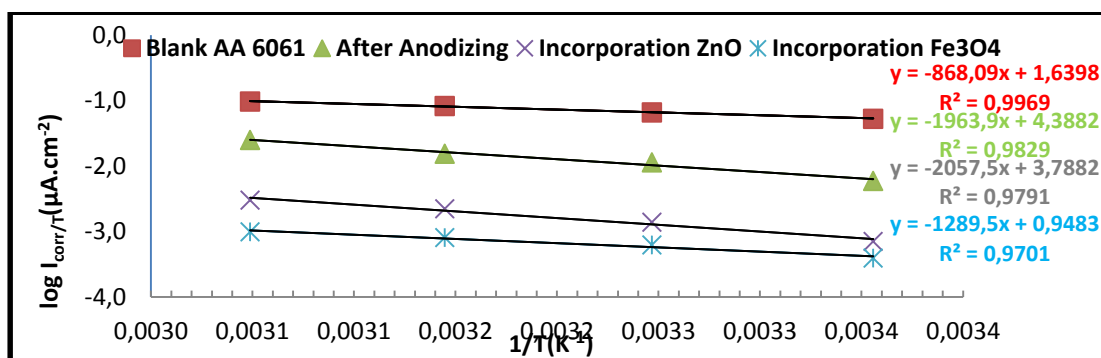


Figure.5. Kinetic and thermodynamic parameters for the corrosion Protective of Aluminum 6061 alloy in seawater at the temperatures range (298-328) K

The following equation may be used to compute the free energy change of the electrochemical corrosion process transition state:

$$\Delta G^* = \Delta H^* - T\Delta S^* \dots\dots\dots (5)$$

ΔG^* values for AA6061 handled with Anodizing and incorporation increased from (66.138 kJ.mol⁻¹) to (71.438 kJ.mol⁻¹), (76.541 kJ.mol⁻¹), and (78.152 kJ.mol⁻¹) with Anodizing, "Anodizing + ZnO incorporation", and "Anodizing+ Fe₃O₄ incorporation" respectively at 298K, indicating a rise in free energy of activation after A6061 surface modified. Anodizing with ZnO incorporation resulted in a larger change in enthalpy, indicating that corrosion requires more energy in this case, and these results are in excellent agreement with the protection efficiency results.

Table 2
Kinetic and thermodynamic parameters for the corrosion Protective of Aluminum
6061 alloy in seawater at the temperatures range (298-328) K

Temp.(K)	1/T(K ⁻¹)	E _{Corr} /mV	I _{Corr} /μA.cm ⁻²	Log I _{Corr}	-ΔG/kJ.mo ⁻¹	ΔH/kJ.mol ⁻¹	ΔS/J.K ⁻¹ .m ⁻¹	Ea/kJ.mol ⁻¹	A Molecule cm ⁻²	
AA 6061	298	0.0034	-	15.73	1.197	66.13	16.621	-0.166	19.220	2.23253E+28
	308	0.0032	-	20.55	1.313	67.80				
	318	0.0031	-	26.3	1.420	69.46				
	328	0.0030	-	31.83	1.503	71.12				
Anodizin g	298	0.0034	-	1.77	0.248	71.43	37.438	-0.144	40.201	1.25054E+31
	308	0.0032	-	3.54	0.549	72.57				
	318	0.0031	-	4.91	0.691	73.70				
	328	0.0030	-	8.23	0.915	74.84				
Anodizin g with ZnO	298	0.0034	-	0.211	-0.676	76.54	38.522	-0.128	41.118	2.31045E+30
	308	0.0032	-	0.483	-0.316	77.81				
	318	0.0031	-	0.711	-0.148	79.09				
	328	0.0030	-	0.992	-0.003	80.36				
Anodizin g with Fe ₃ O ₄	298	0.0034	-	0.117	-0.932	78.15	24.690	-0.179	27.289	4.54147E+27
	308	0.0032	-	0.193	-0.714	79.94				
	318	0.0031	-	0.257	-0.590	81.74				
	328	0.0030	-	0.324	-0.489	83.53				

Kinetic parameters for the corrosion process

Figure (6) represents the corrosion of (blank aluminum, anodized aluminum, anodized aluminum + ZnO Nps, and anodized aluminum + Fe₃O₄ Nps) with the logarithm of current density plotted against reciprocals temperature, can obtain the data in a table (2) and shows the activation energy increased after anodizing Aluminum alloys without and with ZnO and Fe₃O₄, change from (19.220 kJ.mol⁻¹) to (40.201 kJ.mol⁻¹), (41.118 kJ.mol⁻¹) and (27.289 kJ.mol⁻¹) respectively, the activation energy for Aluminum anodized aluminum + Fe₃O₄ was lower than anodized without nanoparticles because the number of corrosion sites on Aluminum anodized surface in presence Fe₃O₄ is decreased, the number of corrosion sites can be indicated by Arrhenius factor (15, 16).

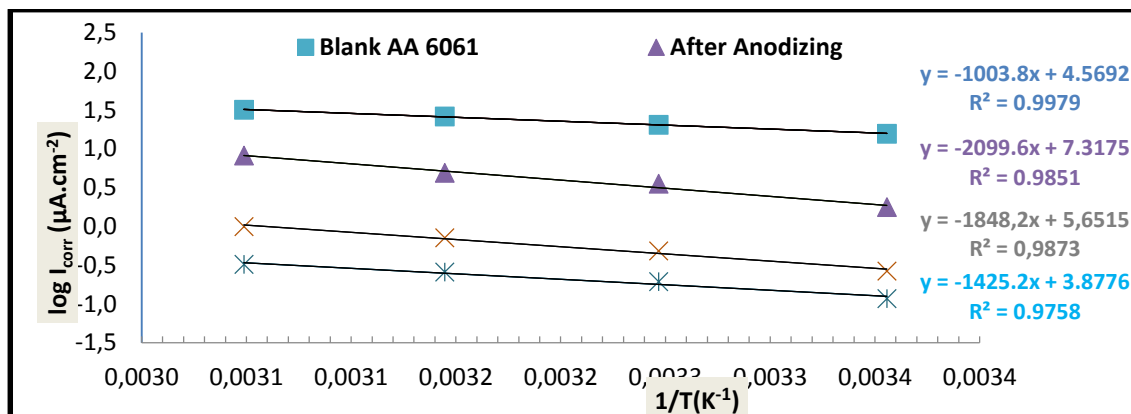


Figure 6. Arrhenius Plot of $\log I_{\text{corr}}$. Versus $1/T$ for the corrosion for Protective Aluminum 6061 alloy in seawater at the temperatures range (298-328) K

Conclusion

In conclusion, the electro-modification of the A6061 surface with anodizing and nanoparticle incorporation provided a better barrier film on aluminum. Anodizing aluminum does not change the corrosion potential but reduces the current density to 88.7% at 298K, and it has significantly raised as the temperature raised. The protection efficiency % PE was observed after AA6061 anodizing, which gave a % PE of 88.7% at 298K. While the best % PE was obtained after AA6061 was incorporated with Fe₃O₄, which gave a % PE of 98.65% percent at 298K. The apparent activation energy of AA6061 is 40.20 kJ/mol while these increases in activation energy result increase in the activation sites and indicated by Arrhenius factor and this increase in Arrhenius factor due to decrease in corrosion rate. The free energy change ΔG^* values for AA6061 that modified with (Anodizing and incorporation); increased from (66.138 kJ.mol⁻¹) to (71.438 kJ.mol⁻¹), (76.541 kJ.mol⁻¹), and (78.152 kJ.mol⁻¹) with Anodizing, "Anodizing + ZnO incorporation", and "Anodizing+ Fe₃O₄ incorporation" respectively at 298K, indicating a rise in free energy of activation after A6061 surface modified. The average partials size of the diameter of formed pores was 215 nm while the average. from XRD data was (19.8 nm). These results qualify our work to be applied in the field of surface modification.

References

1. Khojastehnezhad, V.M. and H.H. Pourasl, Microstructural characterization and mechanical properties of aluminum 6061-T6 plates welded with copper insert plate (Al/Cu/Al) using friction stir welding. Transactions of Nonferrous Metals Society of China, 2018. 28(3): p. 415-426.
2. Salloomi, K.N., Fully coupled thermomechanical simulation of friction stir welding of aluminum 6061-T6 alloy T-joint. Journal of Manufacturing Processes, 2019. 45: p. 746-754.
3. Venukumar, S., et al., Microstructural and mechanical properties of walking friction stir spot welded AA 6061-T6 sheets. Procedia materials science, 2014. 6: p. 656-665.

4. Dorbane, A., et al. Mechanical Response and Evolution of Damage of Al6061-T6 Under Different Strain Rates and Temperatures. in Proceedings of the TMS Middle East—Mediterranean Materials Congress on Energy and Infrastructure Systems (MEMA 2015). 2015. Springer.
5. Shen, D., et al., Microstructure and corrosion behavior of micro-arc oxidation coating on 6061 aluminum alloy pre-treated by high-temperature oxidation. *Applied Surface Science*, 2013. 287: p. 451-456.
6. Hakimizad, A., K. Raeissi, and F. Ashrafizadeh, A comparative study of corrosion performance of sealed anodized layers of conventionally colored and interference-colored aluminum. *Surface and Coatings Technology*, 2012. 206(22): p. 4628-4633.
7. Ghali, E., Corrosion resistance of aluminum and magnesium alloys: understanding, performance, and testing. 2010: John Wiley & Sons.
8. Pornnumpa, N. and M. Jariyaboon, Antibacterial and corrosion resistance properties of anodized AA6061 aluminum alloy. *Engineering Journal*, 2019. 23(4): p. 171-181.
9. Almashhadani, H., Synthesis of a CoO-ZnO nanocomposite and its study as a corrosion protection coating for stainless steel in saline solution. *Int. J. Corros. Scale Inhib*, 2021. 10(3): p. 1294-1306.
10. Kadhim, M.M., et al., Effect of Sr/Mg co-substitution on corrosion resistance properties of hydroxyapatite-coated on Ti-6Al-4V dental alloys. *Journal of Physics and Chemistry of Solids*, 2022. 161: p. 110450.
11. Suman, T., et al., GC-MS analysis of bioactive components and synthesis of silver nanoparticle using *Ammannia baccifera* aerial extract and its larvicidal activity against malaria and filariasis vectors. *Industrial crops and products*, 2013. 47: p. 239-245.
12. AlMashhadani, H.A., Corrosion protection of pure titanium implant in artificial saliva by electro-polymerization of poly eugenol. *Egyptian Journal of Chemistry*, 2020. 63(8): p. 2803-2811.
13. Almashhadani, H.A., et al., Corrosion inhibition behavior of expired diclofenac Sodium drug for Al 6061 alloy in aqueous media: Electrochemical, morphological, and theoretical investigations. *Journal of Molecular Liquids*, 2021. 343: p. 117656.
14. Al-Mashhadani, H.A., et al. Anti-Corrosive Substance as Green Inhibitor for Carbon Steel in Saline and Acidic Media. in *Journal of Physics: Conference Series*. 2021. IOP Publishing.
15. AlMashhadani, H.A. and K.A. Saleh, Electro-polymerization of poly Eugenol on Ti and Ti alloy dental implant treatment by micro-arc oxidation using as Anti-corrosion and Anti-microbial. *Research Journal of Pharmacy and Technology*, 2020. 13(10): p. 4687-4696.
16. AlMashhadani, H.A. and K.A. Saleh, Electrochemical Deposition of Hydroxyapatite Co-Substituted By Sr/Mg Coating on Ti-6Al-4V ELI Dental Alloy Post-MAO as Anti-Corrosion. *Iraqi Journal of Science*, 2020. 61(11): p. 2751-2761.